Single-Shot Multiwavelength Imaging of Laser Plumes

MATTHEW P. NELSON, WENDY C. BELL, MICHAEL L. McLESTER, and M. L. MYRICK*

Department of Chemistry and Biochemistry, University of South Carolina, Columbia, South Carolina 29208

A novel optical approach to single-shot chemical imaging with high spectroscopic resolution is described with the use of a prototype dimension-reduction fiber-optic array. Images are focused onto a 30 × 20 array of hexagonally packed 250 μm o.d. *f*/2 optical fibers that are drawn into a 600 × 1 distal array with specific ordering. The 600 × 1 side of the array is imaged with an *f*/2 spectrograph equipped with a holographic grating and a charge-coupled device (CCD) camera for spectral analysis. Software is used to extract the spatial/spectral information contained in the CCD images and deconvolute them into wavelength-specific reconstructed images or position-specific spectra that span a 190 nm wavelength space. "White light" zero-order images and first-order spectroscopic images of laser plumes have been reconstructed to illustrate proof-of-principle.

Index Headings: **Fiber optics; Chemical imaging; Spectroscopic imaging; Charged-coupled device (CCD); Laser-induced breakdown spectroscopy (LIBS)**.

INTRODUCTION

Most spectroscopic applications involve simultaneous measurement of no more than one or two dimensions of data. Diode arrays can be used to collect one spectroscopic dimension, for example.[1] Charge-coupled device (CCD) arrays can be used to collect two spectroscopic dimensions[2,3] or two spatial dimensions (e.g., a typical video camera), or one of each.[4,5] However, there are applications in which three-dimensional data are useful. Examples include the characterization of the spectroscopy of a laser plume,[6,7] the spectroscopic imaging of composites,[8–10] and the spectroscopy of medical conditions.[11–14]

In this report, we use laser-excited plumes to investigate spectroscopic (also called chemical) imaging. In the past, most such studies have made use of the implicit homoergodic assumption that partial characterization of many laser-ablation plumes is equivalent to complete characterization of a single plume, because the latter measurement presented experimental difficulties.

Applications of laser ablation range from thin-film manufacturing[15–18] to laser surgery.[19–21] Because potential analytical applications of laser plume spectroscopy are complicated by efficiency factors, an understanding of the mechanisms underlying laser plumes may improve analytical precision. Until now, finding a method that can provide spatial, spectral, and temporal information for a single event has been impossible. Yet possible uses of laser plume spectroscopy (equivalently called laser-induced breakdown spectroscopy or laser spark spectroscopy) would appear to require at least information about the size and temperature of a plasma event, as well as the intensity of species-specific emission lines, in order to provide a precise analytical measurement.

Recent efforts using an interferometric spectral-imaging technique have been applied to obtain temporal, spatial, and spectral information about a laser-ablated liquid sample.[22] The technique known as multiple-image Fourier transform spectral imaging (MI-FTSI) utilizes an array of lenslets that create multiple images of the sample phenomena that are superimposed with various path differences in a Michelson interferometer. In Ref. 22, the images were not formed by plasma emissions from the laser plume, but were reflections from sample illumination via a xenon lamp. The authors were unable to obtain images without the lamp. In addition, the discrete values of pathlength difference restrict the spectral resolution of the measurement unless the number of discrete measurements becomes very large.

In this paper we present a novel approach to the single-shot acquisition of spectroscopic imaging data using a two-dimensional array of hexagonally close-packed optical fibers that are reformed into a one-dimensional fiber array at the distal end. An image presented to the two-dimensional proximal end of the fiber array is systematically reordered by row and column in the one-dimensional distal end, and is then injected, in parallel, into a spectrograph for spectroscopic dispersion. The array acts as a dimension-reduction or dimension-transformation device to permit three-dimensional data to be recorded on a two-dimensional detector without loss of spectroscopic resolution. The light-dispersed CCD images then contain both spatial and spectral information that can be extracted and recombined by computer software. In this paper, we demonstrate the potential of the dimension-reduction array by simultaneously acquiring spatial and spectral information from single laser plumes.

EXPERIMENTAL

Fiber Array. A prototype optical fiber array was constructed that consisted of 250 μm o.d. *f*/2 optical fibers

Received 9 June 1997; accepted 27 August 1997.
* Author to whom correspondence should be sent.

0003-7028 / 98 / 5202-0179$2.00 / 0

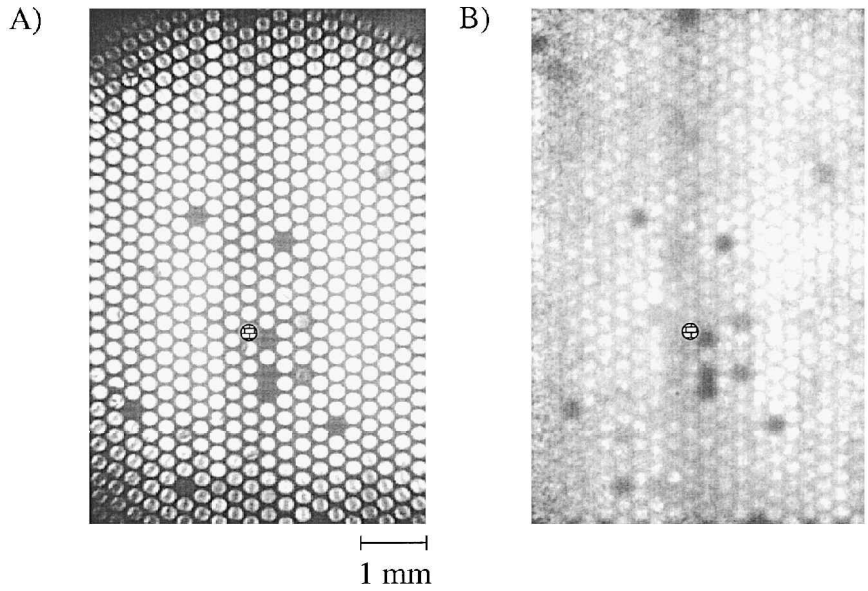

FIG. 1. (**A**) CCD image of 30 × 20 array of hexagonally packed 250 μm o.d. fiber optics imaged with the Chromspec™ CCD camera; (**B**) the same imaged through translucent paper. The "brick-patterned" fiber is the major fiber responsible for the data in Fig. 8 below.

(Polymicro Inc.). The proximal end of the fiber array (Fig. 1) incorporated a 30 × 20 matrix of hexagonally packed fibers that were ordered into a 600 × 1 linear array at the distal end (Fig. 2). Fiber lengths ranged from approximately 4 to 6 in. depending upon orientation in the 600 × 1 linear array. The total length of fiber used in this construction, including excess that was trimmed away, was 200 m. The polyimide jacket was left on the fibers to improve flexibility. The fibers were arranged at the distal end so that adjacent rows of the 30 × 20 matrix were juxtaposed in the 600 × 1 array. The optical fibers were secured to a 7.5 × 5 × 0.125 in. piece of aluminum with 5 Minute® Epoxy (Devcon Corp.). The proximal end of the construct was machined so that a 25 mm television lens (Cosmicar, Inc.) could be threaded in order to focus images onto the 30 × 20 fiber matrix.

The array was constructed as follows: First, a precision clamp was manufactured with a width equal to 30.5 fibers. Up to 90 fibers were loaded into the clamp and compressed, assuming a hexagonally close-packed arrangement. More than 90 fibers at a time resulted in frequent packing flaws. While the fibers were compacted, a coating of polyacrylate superglue was added to the exposed end of the 30 × 3 face. Excess glue on the top and bottom of the segment was removed by brushing with thinner. After drying, the segment was carefully removed from the clamp. When the segments had been prepared in this way, they were stacked together back into the clamp to form a 30 × 20 array. The array was pushed slightly forward to expose enough fiber from the end of the clamp for mounting later, and the clamp was tightened to hold the fibers rigidly for the remaining operations. Near one end of the aluminum support plate a strip of two-sided tape was attached. Layer by layer, the 20 layers were affixed to the tape and fastened in place with individual strips of tape at the extreme end of the aluminum plate. Once all 20 rows were attached, a layer of glue was added to permanently fix them in place. The 30 × 20 end of the array, still in the clamp, was flexed into position at the opposite end of the plate, and a thick layer of glue was added to fix, support, and protect the fibers. A threaded aluminum ring was placed over the exposed two-dimensional end and sealed in place with more glue. Finally, the clamp was removed and a last covering of sealant added to complete the body of the array. Both ends were then trimmed and polished with 3M polishing paper.

Since it would be impossible to completely avoid crosstalk between the fibers on the detector, it was our intent to make adjacent fibers in the 600 × 1 end be fibers highly correlated with one another. The arrangement was not completely achieved, however, due to construction constraints and human error. In some instances, an entire row was flipped in a direction that separated adjacent row end fibers. In addition, the ideal arrangement would have had the fibers in a square-packing arrangement, while the hexagonally close-packed arrangement was used in the actual array for ease of manufacture.

Experimental Optics. The instrumental apparatus is shown schematically in Fig. 3. A 1064 nm Nd:YAG laser pulse (Continuum Surelite I) with a 5–7 ns pulsewidth was deflected at 90° with a 1064 nm YAG laser line coated mirror (Newport Corp.) and focused onto the sample with a 1 in. diameter *f*/4 lens (Newport Corp.). Focal spot size was between 50 and 100 μm in diameter on the basis of burn patterns. The proximal end of the fiber array was positioned so that the television lens attached to it was approximately 4 cm from the sample, the focal plane of the lens being in the center of the plume created by the laser pulse. Facing opposite the television lens of the fiber array was a Chromspec™ CCD camera (Chromex Inc.) thermostated at −20 °C equipped with a 50 mm television lens (Computar Inc.) positioned so that its focal plane was also in the center of the plume, but from the opposite side of the plume. For comparison of the images taken by the fiber array system with the Chromspec™ system, the Chromspec™ images were inverted.

A 1 in. diameter *f*/2 lens was situated approximately

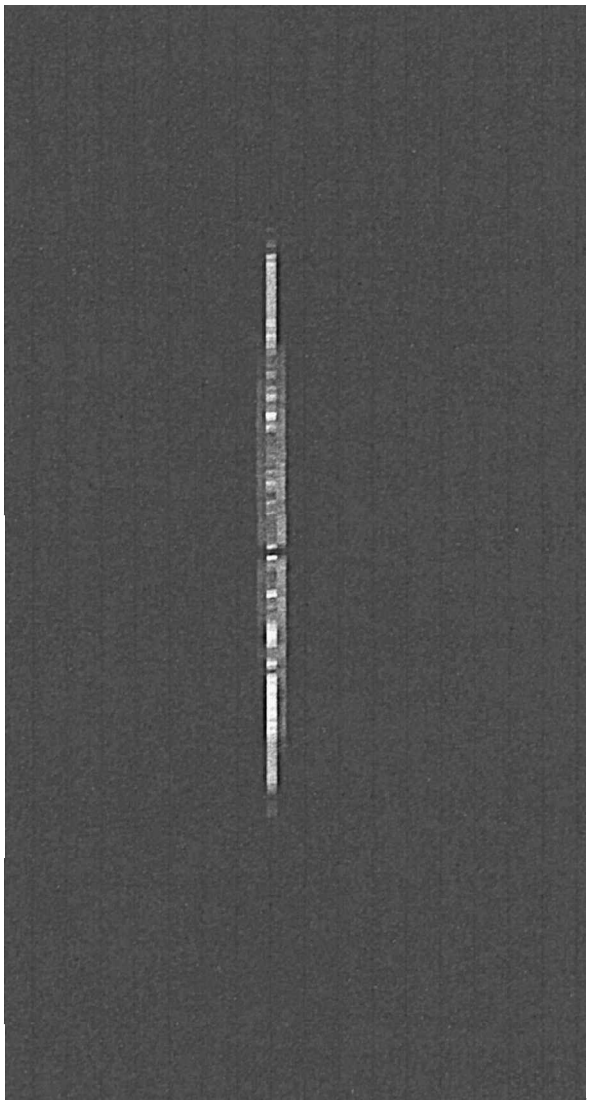

FIG. 2. Image of the 600 × 1 distal end of the array taken with the zero-order grating reflection. The vertical axis corresponds to fiber position in the 600 element array, while the horizontal corresponds to the spatial dispersion direction.

20 in. from the 600 × 1 array side of the dimensional reduction array to produce an effective 0.1× magnification. This arrangement produced an effective slit width of 25 μm with the use of 250 μm o.d. optical fibers and the assumption of perfect imaging. Since our lenses were single plano-convex lenses, we certainly did not achieve this optimum "slit width". The effective slit was located at the focal plane of a single-stage spectrograph (Laser Raman Systems) equipped with *f*/2 optics and a 830 grooves mm^{-1} holographic grating blazed at 812.5 nm (Milton Roy Co.). A thermoelectrically cooled 1100 × 330 pixel CCD camera (Princeton Instruments, Inc.) thermostated at −50 °C was used for detection and controlled with WinSpec software (Princeton Instruments, Inc.) with the use of a 486 IBM-compatible computer. The CCD chip was oriented with the 1100-pixel axis parallel to the 600-fiber distal end of the fiber array and perpendicular to the dispersion direction of the spectrograph.

Again, a serious flaw in this prototype array is apparent: the fibers are too large. To record the 600 250 μm diameter fibers on approximately 600 25 μm-tall pixel rows, we must demagnify the array by a factor of 10. Since the fibers are *f*/2, 1:1 imaging would *f*/#-match the fibers to the spectrograph. Worse, we had no lenses of sufficient diameter to capture the light from so large a source. Consequently, the throughput from the array with the spectrograph was an abysmal 0.01. Smaller fibers would boost this factor by nearly two orders of magnitude. Finally, the spectrograph was not designed for this purpose, and it vignetted the image reaching the detector. We view the results presented as a worst-case scenario.

Software. Software was written for image reconstruction with the use of Labview® 4.0 (National Instruments) augmented by the Concept V.i. virtual instruments for image processing (Graftek). The software prompts the user for information such as starting and ending pixel row values occupied by the array. The program then prompts the user to load a 16-bit CCD image. Once this image is loaded, the user is prompted to load a reference white light image that is used to correct for vignetting caused by the optics of the spectrograph and other optics. New CCD images of the array are then extracted as an array of intensity values that are normalized and multiplied by the inverted, normalized reference image array at the user-specified pixel positions. On the basis of the number of pixels occupied by the array on the CCD chip, the image pixels are interpolated to span 600 image points. The program then cuts and reorders this one-dimensional data array according to the ordering of the rows of the fiber array. When we were dealing with spectroscopic images, a parabolic shape was evident in the atomic lines produced on the detector by the one-dimensional array due to aberrations in the lenses of the spectrograph and imperfections in the array. If the array was not perfectly oriented, some tilt in the spectra was also evident. To correct for this, we incorporated a program routine that fits a third-order polynomial to the pixels with the greatest intensity within a range of user-defined pixel values corresponding to the positions that encompass the parabolic atomic line in another reference image. Rows of pixels are rotated left or right to align them. Figure 4 shows a gray-scale CCD image of the top half of the 600 × 1 distal end of the array taken with the zero-order grating reflection before **(A)** and after **(B)** the third-order polynomial fit correction. The program also contains options that allow for three-dimensional viewing of the reconstructed image as well as multiple color tables for image enhancement. A copy of the program can be furnished upon request.

To summarize, the software corrects for curvature of the spectra, tilt of the array, and vignetting of the image within limits, and makes it unnecessary to exactly fit 600 fiber images onto 600 vertical pixels in addition to reconstructing images.

Sample Setup. White-light reference images were acquired for vignetting correction by diffusing light evenly over the focal plane of the television lens on the fiber array through a piece of white paper.

Array masks were produced by two methods. The first was to block appropriate sections with a 3.66 mm i.d. (5.91 mm o.d.) aluminum washer directly in front of the 30 × 20 array. White light was then used to illuminate the proximal side of the array. To get actual images of

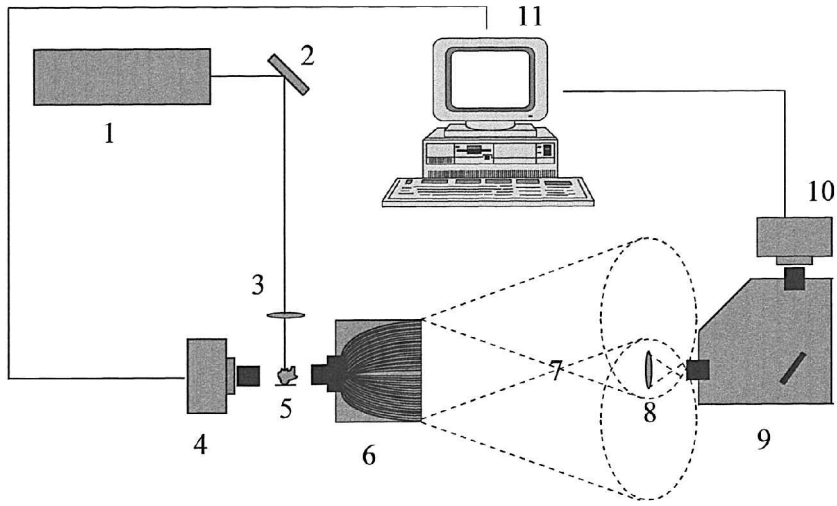

FIG. 3. Diagram of the experimental setup. (**1**) Nd:YAG laser; (**2**) 1064 nm YAG laser line coated mirror; (**3**) *f*/4 plano-convex lens; (**4**) Chromspec™ CCD camera; (**5**) laser plume created on sample surface; (**6**) dimension reduction array; (**7**) illustration of *f*/2 cones of light emerging from the top and bottom fibers of the array; (**8**) *f*/2 plano-convex lens; (**9**) *f*/2 spectrograph; (**10**) Princeton Instruments 100 × 330 pixel CCD camera oriented with the 1100 pixel axis parallel to the 600-fiber distal end of the fiber array and perpendicular to the dispersion direction of the spectrograph; (**11**) 486 IBM-compatible computer.

the focal plane, we used white light to illuminate from the distal 600 × 1 side, and images were captured by using the Chromspec™ CCD camera. In some cases, the blocks were imaged through a piece of white paper in order to visualize the outer edges of the array, which were otherwise darkened due to vignetting. The second method was to image an object at the focal planes of the two television lenses that completely blocked the light from going through it. Laser plumes were imaged with simultaneous capture with the use of both cameras integrating over a time that encompassed the 5–7 ns laser pulse period (approximately 2 to 3 s). We used this approach because we had no simple means of triggering the entire apparatus on the basis of the laser pulse trigger signal. Consequently, our images are not time-resolved.

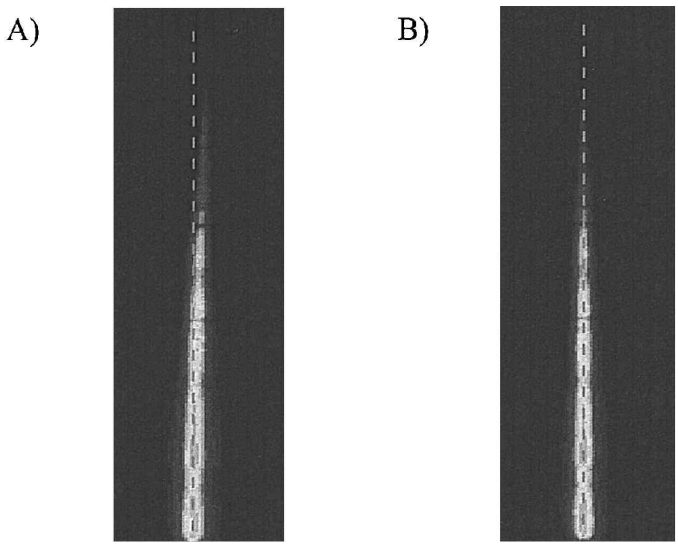

FIG. 4. Gray-scale CCD image of the top half of the 600 × 1 distal end of the array taken with the zero-order grating reflection before **(A)** and after **(B)** the third-order polynomial fit correction, emphasized by a superimposed dotted verticle line.

RESULTS AND DISCUSSION

Dimension-Reduction Optical Fiber Array. Figure 1A shows an actual white-light illuminated image of the 30 × 20 array side imaged with the Chromspec™ CCD camera. Note that approximately 12 of the fibers are not transmitting light due to breaks in the fiber. The vignetting effects from the lens that cause the outer edges of the image to darken with autocontrasting can be minimized by imaging the array through translucent paper (Fig. 1B). Figure 2 shows a Princeton Instruments CCD camera image of the 600 × 1 distal end of the array taken with the zero-order grating reflection. The vertical axis corresponds to fiber position in the 600-element array, while the horizontal corresponds to the spatial dispersion direction. The vignetting of the array by the optics is evident on the ends of the array. This effect is minimized in the reconstructed images by inverting the normalized intensities associated with the zero-order white-light image array and multiplying the array by the normalized array of the image to be reconstructed. This approach gives less emphasis to the intensity of the fibers in the middle of the array and more to those on the ends to correct in software for the optical flaw.

Zero-Order Image Reconstruction. Figure 5 shows an actual image **(A)** and a reconstructed gray-scale image **(B)** of a circular mask, demonstrating the level of image fidelity we have been able to achieve with our less-than-optimum optics. The radial crack in the actual mask is accurately reflected in the reconstructed image, although the crispness of the image is limited by the aberrations of our simple *f*/2 plano-convex front lens. Columns 2 and 11 in the reconstructed image appear to be out of alignment by one pixel. This offset is attributed to imperfect spacing of fibers during the construction of the array. Figure 6 shows an actual image and a gray-scale reconstructed image of a Nd:YAG laser ablation of black electrical tape through to the glue side. This sample was chosen because of the relatively large plume produced during

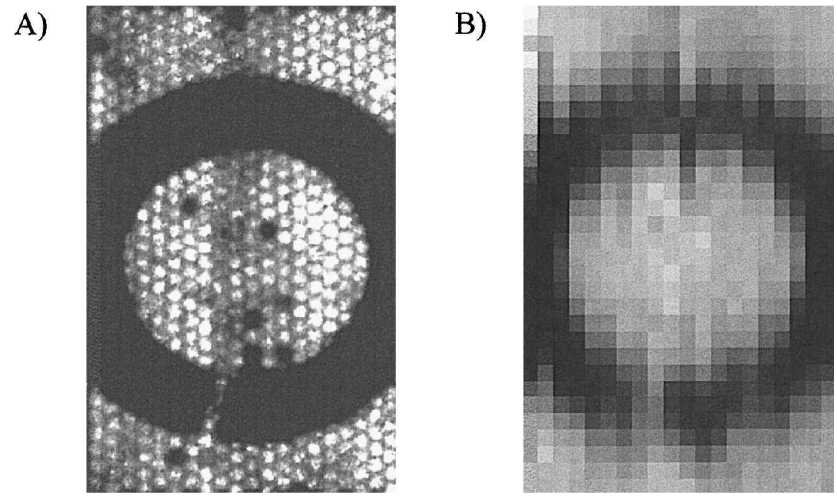

FIG. 5. Actual image **(A)** and reconstructed gray-scale image **(B)** of a circular mask.

the ablation. The actual image has three triangular ghost images in the central portion of the image that are a result of reflections between the internal lens and iris of the Chromspec™ CCD camera. Note the pixels near the top of the reconstructed images in columns 11 and 20 due to blooming of light to neighboring pixels. Because of an error in construction, these fibers from a region distant from the plume center on the two-dimensional side of the array were inadvertently juxtaposed with plume center fibers on the one-dimensional array. Bleed-over from those fibers created the apparent bright spot in an otherwise dark region of the image. These pixels are actually adjacent to the intense pixels near the plume center on the two-dimensional array face but were flipped in the reverse order during the construction of the array. This problem can be resolved by better construction of future arrays.

First-Order Image Reconstruction. Figure 7 shows the first-order CCD image of a mercury calibration lamp imaged through the dimension reduction optical fiber array. The characteristic atomic emission lines at 577.0, 579.1, and 546.1 nm are visible in the image. Figure 8 shows an emission spectrum extracted from a single shot of laser-ablated lead solder taken from a single row of pixels on the Princeton Instruments CCD. These data correspond to the fiber coded in ''brick-pattern'' in Fig. 1. The image was acquired on the fifth pulse in order to avoid surface oxides on the lead solder sample. To demonstrate proof-of-principle, we reconstructed the image from the 722.9 nm lead emission line from the peak pixel column (Fig. 9). This reconstruction can be done for any one of the 329 channels across the CCD image. This single measurement can be used to create complete two-dimensional images of the plume with subnanometer resolution over a 190 nm spectral window. Images based on spectroscopic patterns are also possible.

Despite the imperfect construction of this prototype array and the necessarily imperfect optical train used for these experiments, the promise of this approach for spectroscopic imaging is substantial, even in cases where 329 spectroscopic channels are not needed. To make a quantitative comparison between this method and others that are available, we need only define a few terms and consider examples.

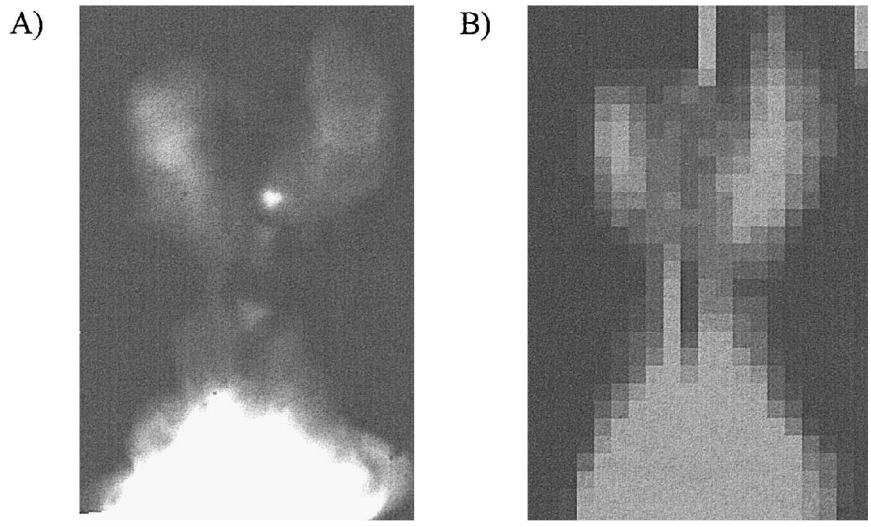

FIG. 6. Actual image **(A)** and reconstructed gray-scale image **(B)** of a Nd:YAG laser ablation of black electrical tape through to the glue side.

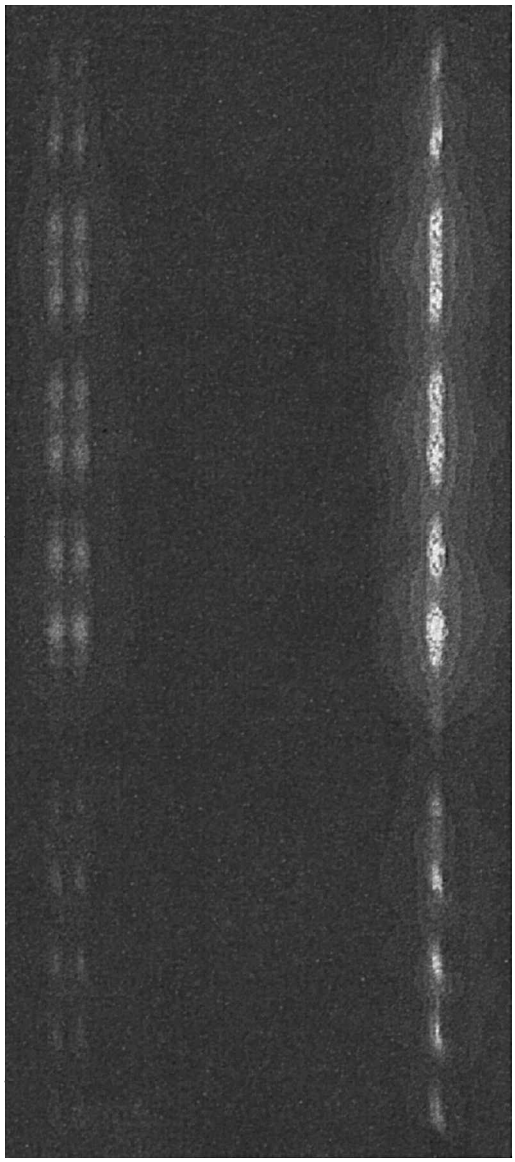

FIG. 7. Cropped first-order gray-scale CCD image of a mercury calibration lamp imaged through the dimension reduction optical fiber array.

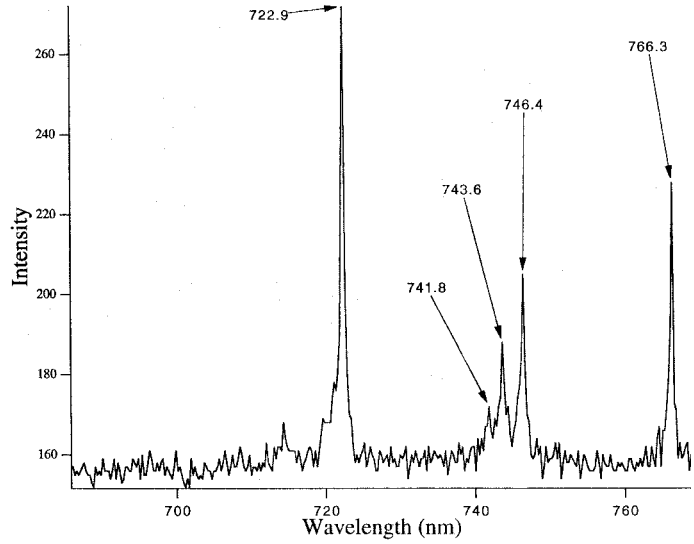

FIG. 8. Emission spectrum extracted from a single shot of laser ablated lead solder taken from a single row of pixels on the Princeton Instruments CCD. These data correspond to the fiber coded in "brick-pattern" in Fig. 1.

Definitions. We will adopt as a definition of chemical or spectroscopic imaging the collection of two spatial dimensions and one spectroscopic dimension of data. A spectroscopic dimension will be defined as a number of wavelength channels greater than the number of significant principal components or patterns in the mathematically untreated (no centering, normalization, etc.) total spectroscopy of a sample. This definition of a spectroscopic dimension is chosen so that the data set will contain sufficient information to deconvolute the composition of the sample and to provide the simplest statistical information for evaluation. By these definitions, no single-wavelength imaging procedure is considered to be chemical or spectroscopic imaging, because the chemical composition cannot be quantified even relatively in such a measurement.

A cursory inspection of spectroscopic imaging methods reveals two limiting cases in which methods should be evaluated. We may characterize these cases as (1) light-limited and (2) scan-speed limited.

The light-limited case will be defined as one in which there are a limited number of photons for measurement regardless of the method chosen. As an example, we can identify Raman imaging: the number of Raman-scattered photons is directly proportional to the number of excitation photons incident. If the excitation source is focused to a single spot, the rate at which scattered photons emerge is high from that spot and zero elsewhere. If the source is spread over the entire image, every spot produces photons at a reduced rate, the rate being inversely proportional to the number of image elements illuminated. Consequently, we should expect that, within limits imposed by power damage thresholds and optical apertures, all experimental methods will perform equally well in this case unless the method "misses" some of the scattered photons.

The scan-limited case will be defined as one in which illumination always encompasses the entire imaged area. Since a laser plume is self-luminous, the laser–plume-imaging situation is an example of this case. We can expect that efficiencies will be greatest for methods that have the highest data acquisition rates in this case.

Numerical Method Comparisons. We can identify four standard data acquisition methods that permit chemical imaging with which to compare the method described herein. These are:

Method 1. Collection of a datum for a specific (X,Y,λ) coordinate, followed by scanning in all dimensions. An example of this method of data collection might be the imaging of a plume with a photomultiplier-based detection system focused on a single point in the plume.[23,24]

Method 2. Collection of a complete spectrum for a single (X,Y) coordinate of the sample, followed by scanning the (X,Y) position within the sample. An example would be scanned-point Ra-

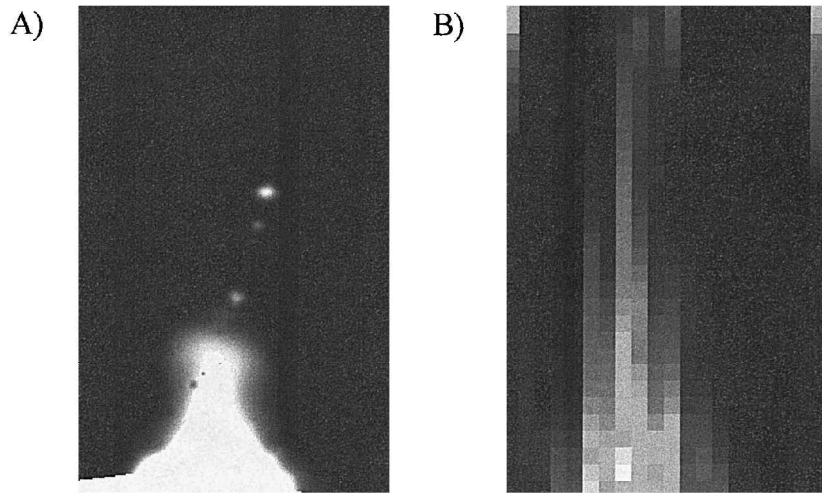

FIG. 9. Reconstructed laser plume image from the 722.9 nm lead emission line from the peak pixel column.

man microscopy with a diode-array or CCD-based detection system.[10]

Method 3. Collection of a complete spectrum for a vertical section of the sample characterized by a single value of X and all values of Y, followed by repetition for different values of X. An example would be line-scan imaging using a CCD array-based detection system.[4–5]

Method 4. Collection of a complete image at a single wavelength channel followed by repetition over the entire wavelength space of the spectroscopy.[25]

There are a variety of permutations of these basic methods, including step-scan Fourier transform imaging and Hadamard transform imaging[25,26] of either the spatial or spectroscopic dimensions. These methods can improve signal-to-noise in (S/N) in measurements, but do not otherwise increase the rate of measurement.

To compare these methods, we will consider the two limiting cases of light-limited or scan-limited measurement. For a light-limited case, we will consider a low-power Raman measurement of a composite material in which single-point (X,Y,λ) measurement will require 1 when the laser is focused at this point. For the scan-limited case, we will consider a measurement of a luminous body in which single-point (X,Y,λ) measurement will require 1. In each experiment we wish to acquire a 20×30 spatially resolved image, and we will further assume for our examples that we must record a minimum of 10 different wavelengths to form a chemical image of the sample—hence the total data array is $20 \times 30 \times 10$. A numerical comparison of the time required to perform a complete experiment by the four methods is presented in Table I for these examples. In this table, Method 5 employs the dimension-reduction array system reported here, and the time between discrete measurements for all methods is assumed to be negligible. As Table I shows, in a light-limited experiment, all the measurements in which the spectroscopic dimension is recorded in a single measurement are equivalent. Only if the complete spectrum is not recorded does a measurement method lag behind in measurement efficiency. On the other hand, scan-limited experiments are quite different in efficiencies.

TABLE I. Numerical comparisons of total experiment time for text example.

Method	Light-limited (s)	Scan-limited (s)
1	6000	6000
2	600	600
3	600	20
4	6000	10
5	600	1

Limitations of Array. A major consequence of the experimental setup is the light losses associated with demagnifying the array. As stated above, nearly 99% of the light is lost from each fiber by using *f*/2 fibers located approximately 20 in. from the 1 in. diameter *f*/2 collection lens. Another obvious limitation of the array is the spatial resolution of the object field. Resolution can be enhanced to a limited extent (e.g., by a factor of 2–4) by using a denser array of fibers. Increasing the number of fibers by a factor of 10 in each dimension would approximate standard video resolution, but would require 60 000 detector rows. An alternative implementation of this system would be to use the data it produces to create a color map that could be superimposed on a high-spatial-resolution gray-scale image of the sample acquired by a standard video camera.

Future Direction and Potential Applications. The dimension reduction array described here enables extraction of spectral and spatial information from an analytical sample in a single shot. Temporal information can easily be obtained by using a pulse amplifier to gate the detector and a digital delay generator to provide timing delays and synchronized gating. Design improvements can be made to increase spatial resolution and allow the optical setup to be more compact, thus improving S/N. It may also be possible to use an alternative mapping of the array from the two-dimensional to the one-dimensional sides that would improve the correlation between adjacent fibers on the one-dimensional side. With these improvements, this method could be used to completely characterize laser plumes spatially, spectrally, and temporally, allowing pa-

rameter optimization to be achieved in fields such as laser surgery and thin-film manufacturing. This technique could be utilized in pattern recognition in numerous biological, medical, and industrial samples by treating each CCD channel number as a spectrum and applying principal component analysis (PCA).[27,28]

CONCLUSION

The work done here shows that spatial and spectral information can be acquired in a single shot by using a dimension-reduction array of optical fibers. Proof-of-principle has been demonstrated with the use of a prototype array consisting of 600 optical fibers. With the aid of computer software written in-house, spatial/spectral information contained in the CCD images has been extracted and transformed into wavelength-specific reconstructed images and position-specific spectra spanning approximately 190 nm with subnanometer resolution. The technique has the advantage of being able to acquire a tremendous amount of pertinent sample information in a single image. The drawbacks of the technique include a trade-off between spectral and spatial resolution. With the proper modifications, however, this methodology can be improved upon and applied to a variety of fields.

ACKNOWLEDGMENTS

M.L.M., M.P.N., W.C.B., and M.L.M. gratefully acknowledge the Army Research Office (Grant Number DAAH04-93-G-0324) and Andrew Crowson for his interest and encouragement.

1. See for example, (a) K. M. Clauwaert, J. F. Van Boxclaer, W. E. Lambert, and A. P. De Leenheer, Anal. Chem. **68,** 3021 (1996); (b) R. A. Desiderio, T. J. Cowles, J. N. Moum, and M. L. Myrick, J. Atmos. Oceanic Tech. **10,** 209 (1993); (c) M. L. Myrick and S. M. Angel, Appl. Spectrosc. **44,** 565 (1990); (d) M. L. Myrick, S. M. Angel, and R. A. Desiderio, Appl. Opt. **29,** 1333 (1990); (e) S. M. Angel and M. L. Myrick, Anal. Chem. **61,** 1648 (1989); (f) S. M. Angel and M. L. Myrick, *Proceedings of SPIE OE/Fibers '89 Symposium*, Boston, Massachusetts (1989).
2. A. R. Muroski, K. S. Booksh, and M. L. Myrick, Anal. Chem. **68,** 3534 (1996).
3. K. S. Booksh, A. R. Muroski, and M. L. Myrick, Anal. Chem. **68,** 3539 (1996).
4. K. Kyle, Lawrence Livermore National Laboratory, private communication.
5. J. L. Wu, *Laser Line-Scan Imaging of Chemical Species with Spectral Similarities Using Multispectral Analysis and PCA*, Honors Thesis, University of South Carolina, Columbia (1996).
6. K. Fushima, M. Badaye, and T. Morishita, J. Appl. Phys. **79,** 3697 (1996).
7. P. Schenck, J. Hastie, A. Paul, and O. Bonnell, Soc. Photo-Opt. Instrum. Eng. **35,** 3199 (1996).
8. R. L. De Leon, W. Wijekoon, U. Narang, M. L. Hall, P. N. Prasad, and J. F. Garvey, J. Phys. Chem. **100,** 10707 (1996).
9. A. J. Wojtowicz, W. Meng, A. Lempicki, G. Beall, D. Hall, and T. Chin, IEEE J. Quant. Electron. **24,** 1109 (1988).
10. C. M. Stellman, K. S. Booksh, and M. L. Myrick, Appl. Spectrosc. **50,** 552 (1996).
11. S. Warren, K. Pope, Y. Yazdi, and A. Welch, IEEE Trans. Biomed. Eng. **42,** 121 (1995).
12. D. W. Hill, Meas. Sci. Technol. **3,** 430 (1992).
13. R. Cubeddu, P. Taroni, and G. Valentini, Opt. Eng. **32,** 320 (1993).
14. F. Konz, J. Ricka, and M. Frenz, Opt. Eng. **34,** 2390 (1995).
15. H. H. Busta, J. Micromech. Microeng. **2,** 43 (1992).
16. M. Morita and T. Ohmi, Jpn. J. Appl. Phys. **33,** 370 (1994).
17. V. I. Makhov, *Proceedings of the 2nd International Vacuum Microelectronics Conference*, Institute of Physics, Bristol, England (1989).
18. D. Baueric, Appl. Phys. A **48,** 527 (1989).
19. G. J. Jake, Med. Instrum. **17,** 407 (1983).
20. M. L. Wolbersht, IEEE J. Quantum Electron. **QE-20**, 1427 (1984).
21. H. Loertscher, W. Q. Shi, and W. S. Grandfest, IEEE Trans. Biomed. Eng. **39,** 86 (1996).
22. A. Hirai, Y. Tsuboi, K. Itoh, and Y. Ichioka, Rev. Sci. Instrum. **67,** 3222 (1996).
23. P. G. Carolan and R. O'Connell, Rev. Sci. Instrum. **66,** 1184 (1995).
24. S. R. Goode and J. N. Emily, Spectrochim. Acta **49B,** 31 (1994).
25. P. J. Treado and M. D. Morris, Appl. Spectrosc. **44,** 1 (1990).
26. D. C. Tilotta, R. M. Hammaker, and W. G. Fateley, Appl. Spectrosc. **41,** 727 (1987).
27. E. R. Malinowski, *Factor Analysis in Chemistry* (John Wiley, New York, 1992).
28. I. T. Joliffe, *Principal Component Analysis* (Springer-Verlag, New York, 1986).